2002 HST Calibration Workshop
Space Telescope Science Institute, 2002
S. Arribas, A. Koekemoer, and B. Whitmore, eds.

NICMOS Grism Calibrations

Rodger I. Thompson

Steward Observatory and Department of Astronomy, University of Arizona, Tucson, AZ 85721

Wolfram Freudling

Space Telescope-European Coordinating Facility, Garching, Germany

Abstract. Installation of the NICMOS cryocooler has restored NICMOS to operational status and has necessitated a recalibration of its primary capabilities including grism observations. This paper describes the results of the recalibration. Most properties of the grisms are essentially unchanged. The principal change has been the different quantum efficiency versus wavelength properties of the detectors. The quantum efficiency is higher at all wavelengths, particularly so at the shorter wavelengths.

1. Introduction

The Near Infrared Camera and Multi-Object Spectrometer (NICMOS) contains three grisms for multi-object infrared spectroscopy with the *Hubble Space Telescope* (*HST*). A grism is a combination of grating and prism that produces a dispersed spectrum with a selected wavelength at essentially the same position as the image of the object in the field of view. The selected wavelength is determined by a combination of the dispersions of the grating and prism. In the case of the NICMOS grisms an interference filter was coated on the front face of the grism to prevent mixing of orders. The front face of the grism is perpendicular to the optical axis of the incoming light and the grating is ruled on the back side of the grism. The ruled faces of the grating grooves are parallel to the front face to provide the proper blaze for the first order. Depending on the location of the object in the image, the zero, first, and second orders can appear in the field of view.

The grisms are in the Camera 3 filter wheel. When in position they are very near the cold pupil of the camera. The optical beam passes through the grism at f/17 as opposed to the usual parallel beam. The effect of the convergent beam on the spectrum is negligible given the large 0.2 arcsecond pixels in camera 3. There are three grisms, G096, G141, and G206 with undeviated wavelengths of 0.94, 1.40, and 2.04 microns.

On March 8, 2002 the NICMOS Cooling System (NCS) was installed on the *HST* to restore NICMOS observational capabilities. The cooler established the final detector (mounting cup sensor) set point temperature on May 10, 2002 at 77.1 degrees Kelvin and the vapor cooled shield at 112 degrees Kelvin. The temperature of the vapor cooled shield will be approximately the temperature of the NICMOS grisms that reside in the camera 3 filter wheel which is thermally tied to the vapor cooled shield. Both of these temperatures are different from the operation in Cycle 7, requiring a recalibration of the grisms. The primary difference in operation is due to the different operating temperature of the NICMOS detectors. The quantum efficiency versus wavelength of each camera 3 pixel must be redetermined to accurately reduce grism spectra. The warmer grism temperature can result in a slightly different dispersion solution. Mechanical distortion created by the instrument warming and subsequent recooling can produce geometric effects such as a change in the tilt of the spectrum on the detector.

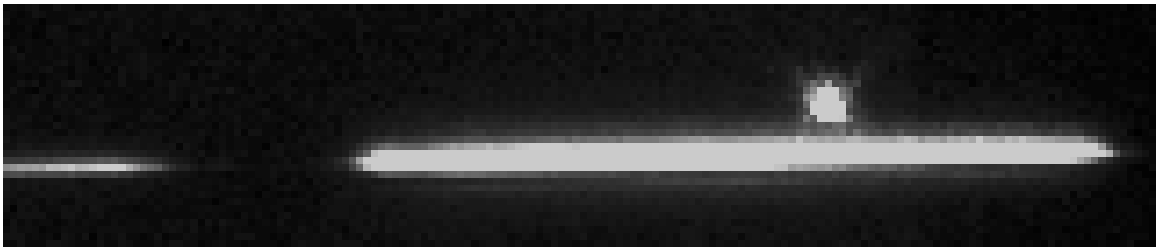

Figure 1. Image and Spectrum Offset.

2. Observations

Proposal 8991 contains all of the grism calibration observations. The solar analog star P330E provides a flux calibrated source to determine the grism-filter efficiency and geometric factors. The compact emission line object Hubble 12 provides multiple spectral lines in each grism for the calculation of the dispersion relation. The NICMOS detectors have significant differences in sensitivity over the area of the detector and within the area of a single pixel. To mitigate this effect images and spectra of each of the two objects were taken at 15 different positions in the camera 3 field of view. The entire first order spectrum is visible at all positions and the zero or second orders are visible at many of the positions.

3. Data Analysis

The basic steps in the data analysis are decomposition of the multiaccum integration into the individual image readouts minus the first read to remove kTC noise, subtraction of the appropriate dark individual readouts for the same multiaccum pattern, correction for linearity, removal of cosmic rays, flat fielding if it is an image but not if it is a spectrum and then correction of known bad pixels. All of this is done with IDL procedures developed by the first author.

4. Geometric Parameters

The geometric parameters for the grisms include the dispersion relation in terms of wavelength per pixel, the angle of the dispersed spectrum relative to the axes of the detector, the offset of the spectrum from the image position and the wavelength of the image position.

4.1. Offset of the Spectrum from the Image and Spectrum Slope

Taking the dispersion direction as the x axis, the image location is offset in the y direction from the spectrum as shown in Figure 1, which is a combination of the F160W image and the G141 spectrum for one of the dither pattern positions. The offset of the spectrum from the image position for the 15 P330E image and spectra was measured for all three grisms by the following process.

The centroids of the F160W image positions were measured with the IDL based procedure Image Display Paradigm (IDP3) developed by the IDT. Note that a check of this procedure relative to several different IRAF procedures revealed significant differences in results on the order of 0.5 pixels. The results from the IRAF procedures were found to vary by the same order of magnitude relative to each other. Because of this the results reported in this report differ from the results used at the Space Telescope–European Coordinating Facility (ST-ECF) for *HST* in Garching, Germany. For a reason not known at the present time the largest differences occur in the IRAF routine IMCENT.

The spectral positions were determined by finding the peak signal position in y for each column of pixels intersecting the first order by gaussian fitting and then finding the best least squares linear fit to those values. In practice this fit always intersected the zero or second order if they were present in the image. The offset was taken as the difference in y pixel values between the centroid of the image and the fit to the spectrum at the x value of the centroid. The slope of the fit also gave the slope of the spectrum relative to the x axis of the detector in y pixels per x pixel. The angle of the spectrum is taken as positive for a counter clockwise rotation. The values of the parameters are given in Table 1. The quoted standard deviations are only from the statistics of the 15 fits.

Table 1. NCS Era Grism Offset and Slope Parameters

Grism	Offset	Offset std dev	Slope	Slope std dev	Angle in Degrees
G096	−4.3	0.4	0.054	0.003	3.1
G141	−6.7	0.4	0.013	0.003	0.73
G206	−2.0	0.4	0.023	0.003	1.3

4.2. Grism Dispersion Relations

The line spectra of Hubble 12 defined the spectral dispersion relation for each grism. The IDL procedure for determining the dispersion assumes that the dispersion relation is linear. This assumption was checked against the observed lines and appears to be accurate within the spectral resolution of the grisms. The procedure takes three prominent and widely spaced lines in each spectrum and finds the best fit using the IDL function POLY_FIT. Table 2 gives the vacuum wavelengths of the lines used in the analysis. The dispersion solution is for vacuum wavelengths.

Table 2. Wavelengths in Microns of the Lines Used in the Dispersion Solution

Grism	Line 1	Line 2	Line 3
G096	1.0832	1.00507	.953461
G141	1.8756	1.28216	1.0832
G206	2.16609	2.0581	1.8756

Note that adjacent wavelength grisms have a line in common to make sure the dispersion solutions match across grism boundaries. An interactive program displays each of the 15 Hubble 12 spectra for a given grism and asks the operator to mark the position of the 3 lines used for the dispersion solution. The line center is found by fitting a Gaussian to the line using the IDL function GAUSSFIT. The center wavelength (the constant) and the dispersion (the slope) are the averages of the 15 measurements and the standard deviation is calculated from the scatter of the measurement values by the IDL function MOMENT. Table 3 shows the results of the measurements. Note that the standard deviation is from the measurements only and does not reflect any possible systematic errors. Only the first order dispersion was measured. The second order should be 1/2 of the dispersion of the first order giving spectra at twice the resolution of the first order. Table 4 gives the regions of the zero, first, and second orders relative to the image position which marks the center wavelength. None of the positions of the spectra were far enough offset to see the long wavelength end of the second order, therefore those positions are upper limits on the extent. Note that the second order fades toward the long wavelength end as the angle of dispersion get further from the blaze angle.

Table 3. Dispersion Solutions for the First Order of the NICMOS Grisms

Grism	Center Wavelength (microns)	Center Wavelength Std. Dev	Dispersion (microns/pixel)	Dispersion Std. Dev.
G096	0.9415	0.002	−0.00552	0.0001
G141	1.396	0.001	−0.008016	5×10^{-6}
G206	2.039	0.001	−0.011353	4×10^{-5}

Table 4. Pixel Positions for the Grism Orders

Grism	Zero	First	Second
G096	+163–+167	−46–+27	−110–< −184
G141	+165–+170	−65–+40	−91–< −184
G206	+166–+173	−43–+58	−57–< −184

Using the dispersion solutions listed in Table 3 the wavelengths of the observed spectrum of Hubble 12 were calculated. Figure 2 through Figure 4 show the observed grism spectrum with the higher resolution ground based spectra overplotted. The ground based spectra in the J, H, and K bands are from Luhman & Rieke 1996 and the shorter wavelength spectra are from Rudy et al. 1993. Since the Rudy data was not available in digitized form, narrow triangular lines were just placed at the wavelengths of the observed lines in the published line list, adjusted to vacuum wavelengths.

5. Efficiency Calibration

The second part of the grism calibration is a determination of the efficiency. The observed signal for a pixel in the spectrum is given by

$$S(\lambda) = F(\lambda)GE(\lambda)FE(\lambda)QE(\lambda) \quad , \tag{1}$$

where $F(\lambda)$ is the object flux in photons per second, $GE(\lambda)$ is the grism efficiency, $FE(\lambda)$ is the filter efficiency and $QE(\lambda)$ is the quantum efficiency of the pixel. Since the filter is applied directly to the front face of the grism it is combined with the grism efficiency for a total grism efficiency such that

$$G(\lambda) = GE(\lambda)FE(\lambda) \tag{2}$$

5.1. Input Spectrum

The solar analog P330-E provides the known input flux and spectrum $F(\lambda)$. The detailed solar spectrum (Wallace, Hinkle & Livingston 1993, Livingston & Wallace 1991) is matched to the fluxes and slopes of ground based spectra of P330-E taken by Marcia Rieke (unpublished) and the NICMOS calibrated fluxes of P330-E. This detailed spectrum is then convolved with the NICMOS Camera 3 PSF and grism spectral resolution to provide the input spectrum.

5.2. Pixel Quantum Efficiency

The remaining task is determination of the quantum efficiency of each pixel in the Camera 3 array as a function of wavelength. This is done using the Camera 3 narrow band filter flat

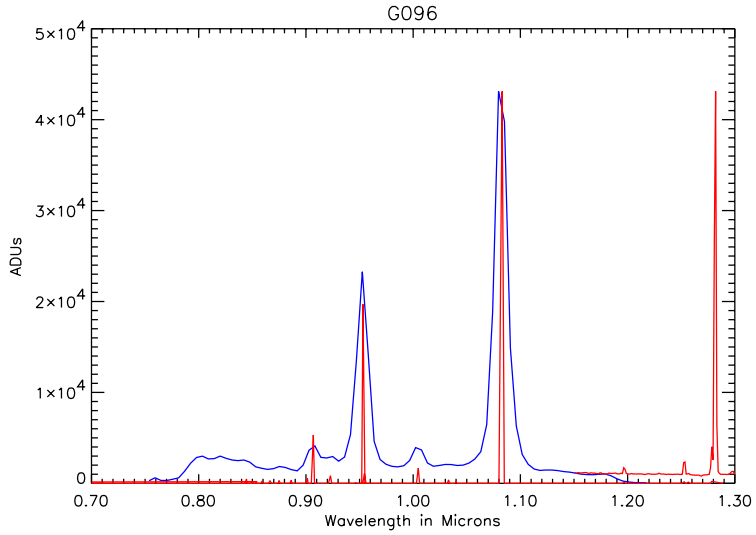

Figure 2. G096 Spectrum of Hubble 12.

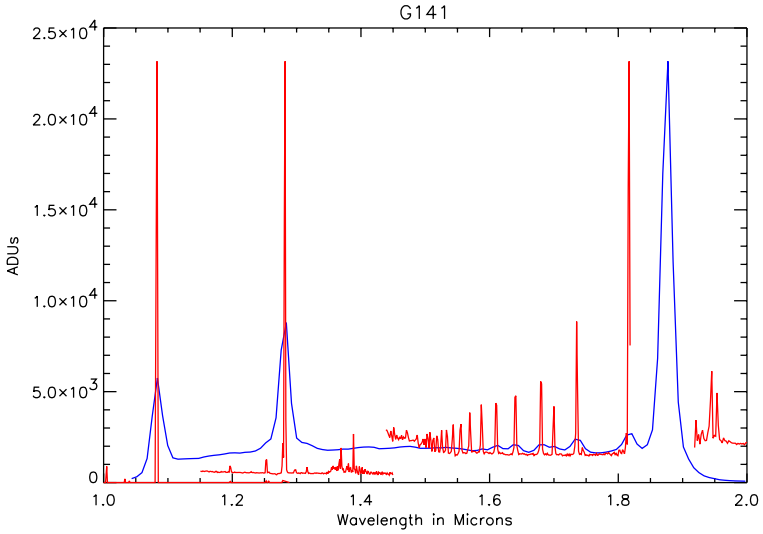

Figure 3. G141 Spectrum of Hubble 12.

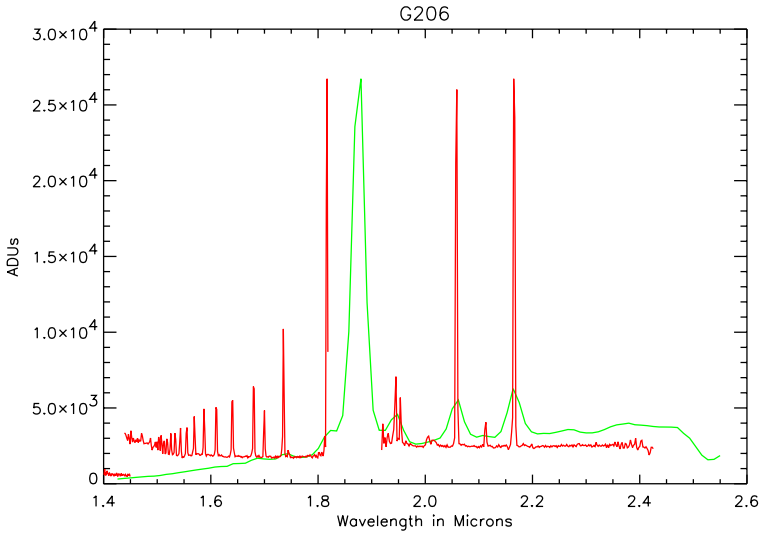

Figure 4. G206 Spectrum of Hubble 12.

fields. The flat fields created by the IDT have a median of 1 and are multiplicative, i.e., the image is flattened by multiplying by the flat field. The procedures for creating the flat fields are covered in Section 5.3.

The median response in Janskys per ADUs/sec for each flat field has been measured in the photometric recalibration of NICMOS. This data has been analyzed by Marcia Rieke and Table 5 gives the median response for the Camera 3 narrow band filters.

Table 5. Camera 3 Narrow Band Filter Responses

Filter	Janskys/(ADU/sec)
F108N	1.01E-04
F113N	8.57E-05
F164N	3.99E-05
F166N	4.28E-05
F187N	3.86E-05
F190N	3.89E-05
F196N	3.65E-05
F200N	3.58E-05
F212N	3.65E-05
F215N	4.03E-05

For each pixel the median responses are divided by the flat field value to get the response of the pixel at the narrow band wavelengths. The responses are then fit with a quadratic function to provide the response of the pixel with wavelength by an IDL procedure.

This procedure does not fit the long wavelength roll off of the detector since none of the narrow band filters fall at those wavelengths and the broad band filters are too broad to measure it. The only narrow band data that measure the roll off are from the laboratory testing done at the University of Arizona before flight. The G206 grism is the only grism that includes the roll off. For that wavelength region the measure preflight roll off is matched to the current response at 2.44 microns to provide the roll off. More accurate determination

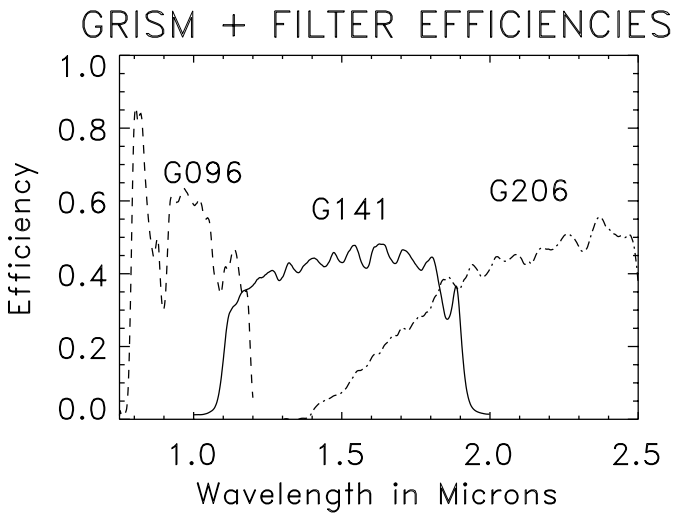

Figure 5. The NICMOS Grism Efficiencies.

can be achieved by using the G206 spectra of P330-E but only for those pixels that happen to lie in that part of the spectrum.

5.3. Camera 3 Narrow Band Filter Flat Fields

All of the Camera 3 narrow band filter flat field observations used in this analysis come from Proposal 9557. The reduction procedure for the individual observations is the same as described in Section 3.0 with two exceptions. First the flat field correction step is obviously skipped. The second exception has to do with the nature of the data. The observations in all of the data sets were driven to extremely nonlinear regions and often to saturation. Since the linearity corrections for the NCS era have not yet been developed it was not possible to correct for nonlinearity. Instead, the cosmic ray correction procedure, which also finds the signal rate, was limited to only the linear regions. This was done with the special cosmic ray correction procedures that accept a parameter indicating how many reads to eliminate from the analysis. This parameter was determined by individual examination of the signal growth in each filter.

After the individual observations were reduced the final flat field was created by taking the median of all of the images, taking the reciprocal of all of the values, and setting the median of the result equal to 1.0. Flat fielding is then accomplished by multiplying an image by the flat field.

5.4. Derived Grism Efficiency Functions

The calculated grism efficiencies are shown in Figure 5 for each of the grisms. The high frequency structures in the efficiency are due to the interference filters.

5.5. Intrapixel Sensitivity

It is well known that the sensitivity of the NICMOS detector array pixels is not constant across the face of the pixel. The sensitivity decreases toward the edges of the pixel. Although not confirmed by experiment it is probable that the degree of sensitivity decrease varies from pixel to pixel. There are various methods to correct for this problem depending on the nature and signal to noise of the spectrum. The efficacy of the various methods has been debated and it is not clear which method works the best. The spectra used in this

analysis have not been corrected by any of these methods. Instead we have dithered the observations to 15 different positions and have used a final spectrum that is the median of the 15 individual spectra to mitigate the effect of intrapixel sensitivity.

6. Calibration Data

All of the NICMOS grism calibration results have been provided to the Space Telescope Science Institute (STScI) for inclusion in their data base. Inquiries about grism calibration or data reduction should be directed to either STScI or the Space Telescope-European Coordinating Facility (ST-ECF). The ST-ECF maintains a NICMOS grism data reduction program called NICMOSlook which can be obtained from the ST-ECF at http://stecf.org/nicmoslook. The current version is 2.12.0. The distribution of NICMOSlook includes calibration data compatible with the results presented here.

Acknowledgments. This work is supported in part by NASA grant NAG 5-10843. This work utilized observations with the NASA/ESA *Hubble Space Telescope*, obtained at the Space Telescope Science Institute, which is operated by the Association of Universities for Research in Astronomy under NASA contract NAS5-26555.

References

Livingston, W. & Wallace, L. 1991, N. S. O. Technical Report #91-001, National Solar Observatory, National Optical Astronomy Observatories, Tucson, AZ 85726

Luhman, K. L. & Rieke, G. H. 1996, ApJ, 461, 298

Rudy, R. J., Rossano, G. S., Erwin, P., Puetter, R. C., & Feibelman, W. A. 1993, AJ, 105, 1002

Wallace, L., Hinkle, K., & Livingston, W. 1993, N. S. O. Technical Report #93-001, National Solar Observatory, National Optical Astronomy Observatories, Tucson, AZ 85726